FULL PAPER

Rigidity-Patterned Polyelectrolyte Films to Control Myoblast Cell Adhesion and Spatial Organization

Claire Monge, Naresh Saha, Thomas Boudou, Cuauhtemoc Pózos-Vásquez, Virginie Dulong, Karine Glinel, and Catherine Picart**

In vivo, cells are sensitive to the stiffness of their microenvironment and to the spatial organization of the stiffness. In vitro studies of this phenomenon can help to better understand the mechanisms of the cell response to spatial variations of the matrix stiffness. Here, polelyelectrolyte multilayer films made of poly(L-lysine) and a photoreactive hyaluronan derivative are designed. These films can be photo-crosslinked through a photomask to create spatial patterns of rigidity. Quartz substrates incorporating a chromium mask are prepared to expose selectively the film to UV light (in a physiological buffer), without any direct contact between the photomask and the soft film. It is shown that these micropatterns are chemically homogeneous and flat, without any preferential adsorption of adhesive proteins. Three groups of pattern geometries differing by their shape (circles or lines), size (from 2 to 100 μm), or interspacing distance between the motifs are used to study the adhesion and spatial organization of myoblast cells. The results pave the way for the study of the different steps of myoblast fusion in response to matrix rigidity in well-defined geometrical conditions.

1. Introduction

Cells are mechanosensors that can signal via the trans-membrane receptors integrins to probe their environment and send signals in a bidirectional manner, a process called outside-in and inside-out signaling.[1] Moreover, it is acknowledged that the stiffness of a natural matrix plays a role in physiological[2] and pathological processes, such as morphogenesis and wound healing,[3] cancer metastasis[4] and inflammation.[5] The importance of the mechanical properties of a matrix has been shown in vitro using model synthetic or natural gels of well-defined properties.[6] Substrate stiffness influences numerous cellular processes from adhesion,[7] migration[8] to proliferation and differentiation.[9,10] Although the coating of synthetic materials by extracellular matrix proteins can influence the nature of the integrin receptors engaged and the ultimate commitment of the cells[11,12] there is now a scientific consensus on the fact that cell sensing, substrate mechanics and force development play a key role in cell spreading and in the formation of focal adhesions.[1] Whereas increasing stiffness enhances adhesion, spreading and proliferation of many cell types[9,10,13] and facilitates tumor growth,[4] compliant substrates appear to promote branching of neurons[14] or albumin secretion by hepatocytes.[15] The mechanism by which cells transduce alterations in substrate stiffness is not fully understood, but it has been shown that cells attached to stiffer matrices generate stronger contractile forces through acto-myosin interaction and cytoskeletal organization, which lead to the formation of larger, more stable focal adhesion complexes.[16] Recently, it was suggested that local variations in stiffness and not stiffness alone influence cell behavior.[17] Indeed, in their in vivo environments, cells are subjected to variations of stiffness at interfaces, e.g., bone connection to cartilage[18] or to muscle.[19] Such a spatial stimulation has first been introduced in vitro by Wang and co-workers[8] to investigate the migration of fibroblasts at the boundary between a soft and a stiff polyacrylamide (PA) gel. These authors introduced the concept of durotaxis, i.e., cell migration from the softer to the stiffer region of the matrix. Various strategies have subsequently been developed to investigate the cell response to a gradient in mechanical properties, mostly using 2D PA gels,[17,20–22] polydimethylsiloxane (PDMS)[23–25] or poly(ethylene glycol) (PEG) gels.[26,27] PA gel rigidity is usually varied by a photo-polymerization process using a patterned photomask[17,22] to form several linear gradients of several millimeter in length with a magnitude of few to several tens of kPa/mm.[17,20] Such stiffness gradients exhibit smooth boundaries and cells were shown to migrate toward stiffer regions of the PA gels. Microfluidics technology was also

Dr. C. Monge, N. Saha, Dr. T. Boudou, Prof. C. Picart
CNRS-UMR 5628
Laboratoire des Matériaux et du Génie Physique
CNRS et Institut Polytechnique de Grenoble
Université de Grenoble
3 parvis L. Néel, F-38016 Grenoble, France
E-mail: Catherine.picart@inp-grenoble.fr
N. Saha, Dr. C. Pózos-Vásquez, Dr. K. Glinel
Institute of Condensed Matter & Nanosciences
Bio & Soft Matter division
Croix du Sud 1, box L7.04.02, B-1348 Louvain-la-Neuve, Belgium
E-mail: Karine.glinel@uclouvain.be
Dr. V. Dulong
Laboratoire Polymères
Biopolymères, Surfaces, CNRS-UMR 6270
Université de Rouen
Bd Maurice de Broglie, F-76821 Mont Saint Aignan, France

DOI: 10.1002/adfm.201203580

© 2013 WILEY-VCH Verlag GmbH & Co. KGaA, Weinheim

combined to photo-polymerization to create 2D PEG hydrogels showing a spatial gradient in stiffness.[26,28] Using square zones of stiffer PDMS in a softer PDMS area, Chen and co-workers[24] showed that sharper gradients of rigidity could be obtained with a spatial resolution of 10 μm. They observed that cells accumulated over the stiffer parts in about 2 days.

Although substrates based on synthetic materials such as PA, PEG and PDMS have been extensively developed to investigate cell behavior, they show some drawbacks that limit the understanding of the influence of the substrate stiffness on cell response. Notably, the potential toxicity of the precursors used for their preparation precludes their in vivo application. Moreover, a protein coating, typically type-I collagen[17,22] or fibronectin,[24] has to be deposited onto these synthetic substrates before cell seeding, which adds a further step in the material preparation and impacts the physicochemical properties of the bare material.

Several technical challenges also remain. Notably, besides stiffness, crosslinking chemistry can also alter the internal structure and surface topology of the hydrogels, especially the adsorption of adhesive proteins.[6,12]

In this context, the development of substrates of controlled rigidity based on biocompatible and bioadhesive materials which mimic extracellular matrices (ECM) is of great interest. In search for engineering micropatterns of such natural materials, Kawano et al. recently used photo-crosslinkable styrenated gelatins.[29] These gels were prepared with a boundary of 50 μm and a gradient slope of 30–40 kPa/50 μm. These authors showed that the number and size of focal adhesions were distributed asymmetrically across the elasticity boundary. However, a topographical variation of 10 μm was observed between the soft and stiff adjacent zones due to swelling discordance across the boundary. Such topographical variation may impact cell behavior.

Polyelectrolyte multilayer films (PEMs) assembled in a layer-by-layer (LbL) fashion[30] are increasingly used to prepare thin films with well-controlled mechanical and biochemical properties. The main asset of PEMs is their versatility with a large choice of building blocks, assembly conditions (pH, ionic strength) and post-processing treatments. Biocompatible PEM films containing biopolymers are an interesting route for future use in the field of tissue engineering[31,32] and as surface coatings of biomaterials.

Besides ionic crosslinking obtained by pH adjustment, which can lead to differences in mechanical properties,[33] additional crosslinking of PEM films can be achieved by three major routes: i) thermal crosslinking,[32] ii) chemical crosslinking including use of a water soluble carbodiimide EDC,[34] and iii) photo-crosslinking by embedding a photo-crosslinkable polyelectrolyte in the PEM film.[35,36] Using covalent amide crosslinking between carboxylic groups of hyaluronan (HA) and amine groups of poly-L-lysine (PLL), we previously demonstrated that the stiffness of (PLL/HA) films can be tuned from 5 kPa to 500 kPa.[37] Moreover, we showed that this film stiffness plays an important role in the adhesion of chondrosarcoma and myoblast cells[37] as well as in their differentiation in myotubes.[38] Indeed, myoblasts are known to be responsive to substrate stiffness.[9,38,39] Nevertheless, chemical crosslinking can only be used to create homogeneously crosslinked films with a given rigidity. Recently, we showed that the stiffness of photo-crosslinked (photo-CL) biopolymeric films made of PLL and of HA grafted with a vinylbenzyl group (HA-VB) can be modulated by varying the grafting degree of the VB group and the exposure time to UV light.[36] Using ≈1 μm thick films, we showed that C2C12 myoblasts spread and proliferated more on stiffer films after 72 h of culture whereas cells on native films kept a round morphology and did not proliferate.

Although preparation of PEMs with spatially controlled photo-crosslinking has been reported to create patterned Bragg mirrors,[35] only one study by Chien et al.[40] explored the potentiality of photo-CL synthetic films based on PAA conjugated with 4-azidoaniline to control cell adhesion. They used an alkaline solution to remove the uncrosslinked areas and cells were let to adhere on the underlying bare substrate. In this case, the photo-CL films served as a physical barrier between cells and as a non-adhesive background.

From these first studies, our challenge was to elaborate flat and chemically homogeneous substrates based on biopolymers mimicking the ECM, with a spatially tunable stiffness and no additional surface biofunctionalization. To this end, we engineered spatial micropatterns of rigidity using photo-crosslinkable (PLL/HA-VB) films to investigate cell positioning in response to spatial variations in stiffness. We developed a protocol to photo-pattern the biopolymeric films in a non-invasive manner, i.e., without pressing a photomask on the film surface and thus avoiding potential damage of the film surface. Instead, the polyelectrolyte multilayer was deposited on a transparent substrate incorporating a patterned photomask which allowed exposing selectively the film to the UV light (**Scheme 1**). Such a process allowed the preparation in a physiological solution of photopatterned PEM films showing a lateral variation of stiffness with a resolution of ≈1 μm. We investigated the adhesion and spatial organization of myoblasts seeded on micropatterns of various shapes and sizes.

2. Results

2.1. Influence of Film Stiffness on the Bioadhesive Properties of (PLL/HA-VB) Films

The photo-crosslinking reaction occurring in (PLL/HA-VB) films under UV exposure results in the formation of C-C bond between vinylbenzyl groups, which progressively disappear with the exposure duration as previously demonstrated by UV spectroscopy.[35,36] The reaction was shown to be completed in ≈30 min.[36] It resulted in a minimum variation of the film chemistry, which was also confirmed by FTIR spectroscopy (data not shown). The Young's moduli of the films measured by AFM nanoindentations were 135 ± 30 kPa for photo-CL films and 25 ± 10 kPa for non-crosslinked (NCL) films.[36]

Myoblasts responded to homogeneously photo-CL films by adhering, spreading and proliferating (ref. [36] and **Figure 1**A). They exhibited a characteristic fibroblastic morphology[41] with the presence of actin stress fibers (data not shown). A full

© 2013 WILEY-VCH Verlag GmbH & Co. KGaA, Weinheim

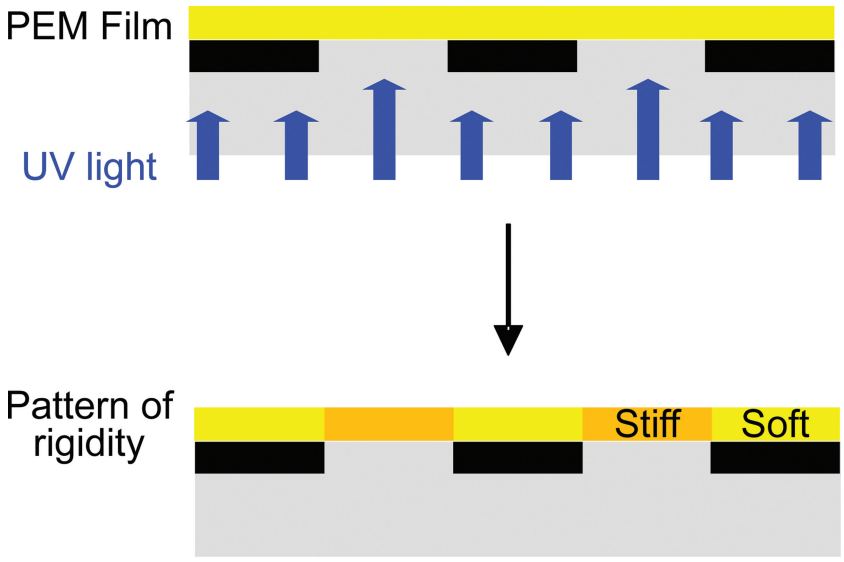

Scheme 1. Preparation of the photo-atterned polyelectrolyte multilayer films. The (PLL/HA-VB)$_{12}$ multilayer film is deposited onto a transparent quartz substrate incorporating a chromium grid. The film is always immersed in a physiological buffer. UV light ($\lambda = 254$ nm) is sent to the film by the bottom of the quartz slide, allowing selective photoirradiation of the film. This leads to the formation of a micropattern of rigidity with softer/stiffer motifs.

coverage of the surface was obtained in 72 h. Conversely, on NCL films, myoblasts were round and tended to form clusters, a phenomenon that was still observed after 72 h of culture (Figure 1A). As cell culture over 3 days is performed in a serum containing medium, i.e a medium containing proteins, we further assessed whether serum proteins may impact cell response to film stiffness. We selected fibronectin (FN) as a major adhesive protein and tested whether its adsorption on the films played a role in the cell response. C2C12 myoblasts were cultured on NCL and photoCL films coated with FN (Figure 1B). FN adsorption did not affect the initial spreading of cells on NCL films and myoblasts were still round and poorly spread. Furthermore, on photoCL films, the presence of FN only slightly enhanced early adhesion: cell confluence was reached after 48 h in growth medium (GM) on FN-coated photoCL films instead of 72 h on photoCL films without FN pre-coating (Figure 1B versus A).

Indeed, we quantified FN adsorption onto the photoCL and NCL films (Figure 1C,D) by using fluorescently labeled fibronectin (FN-FITC). Both fluorescence microscopy (Figure 1C and Figure SI1, Supporting Information) and fluorescence spectroscopy (Figure 1D) conformed that similar amounts of FN-FITC were adsorbed on both NCL and photoCL films. In addition, we confirmed that pre-adsorption of the serum-containing growth medium on the film for 24 h did not change the cell response to film stiffness (Figure SI 2, Supporting Information). Thus, FN or serum pre-coating did no overcome the effect of the film softness of NCL films but had a slight synergistic effect on stiffer films by enhancing cell spreading.

All together, these data showed that protein adsorption from the serum is not a major parameter in the cell response to film stiffness. In the following, all the experiments were done on PEM films in the presence of serum but without FN pre-coating.

2.2. Elaboration and Characterization of Photopatterned Multilayer Films

In our initial trials, the micropatterned photo-CL films were prepared according to the usual photolithography procedure by pressing a photomask directly onto the LbL films while exposing the films to the UV light. However, the surface of the resulting films presented some damages and the process was not reproducible. For this reason, an alternate protocol avoiding contact between the PEM film and the photomask was designed. Transparent substrates incorporating a metal grid playing the role of a photomask were prepared (Scheme SI3, Supporting Information). Experimentally, a 100 nm-deep grid was etched in one face of a fused silica substrate by photolithography and silica etching; a chromium layer of 100 nm thickness was then deposited in the etched recesses Then, the modified surface was coated by a very thin layer of HSQ resin, which upon curing transformed to a silicon oxide layer covering the chromium grid and smoothing the external surface of the substrate. Substrates incorporating chromium grids of various design were prepared to produce different patterns (**Table 1**). After the deposition of the PEM onto the substrate, the photo-crosslinking was performed by immersing the film upside down in buffer solution and exposing it to UV light (Scheme 1). This protocol prevented any contact between the photomask and the polyelectrolyte film, thereby preserving its physical integrity.

Atomic force microscopy (AFM) images of photo-patterned (PLL/HA-VB)$_{12}$ films recorded in liquid are shown in **Figure 2**.

The topography image (Figure 2A) revealed the presence of the micropatterns. In fact, a slight and progressive variation of the film thickness between photoCL and NCL regions with a height decrease of ≈25 ± 5 nm (counted for 15 different micropatterns) over a lateral distance of ≈600 nm was observed. This slight difference in height probably resulted from a slight shrinking of the photoCL areas during the photocrosslinking process.[35] In addition, the variation of rigidity between the crosslinked features and the non-crosslinked background was confirmed by quantitative AFM force mapping (Figure 2C,D). Three representative profiles for E_0 obtained on different patterns showed that a mean E_0 of ≈150 kPa was measured for the photo-CL part as compared to ≈30 kPa for the NCL one (Figure 2D). Altogether, these observations confirmed the presence of the micropatterns of stiffness.

2.3. Myoblast Adhesion and Organization on Photopatterned Films

To assess whether cells are sensitive to the micropattern of rigidity, C2C12 cells were seeded on photo-patterned (PLL/HA-VB)$_{12}$ films. Three groups of pattern geometries differing by their shape (circle or line), size (from 2 to 100 μm) or by

© 2013 WILEY-VCH Verlag GmbH & Co. KGaA, Weinheim

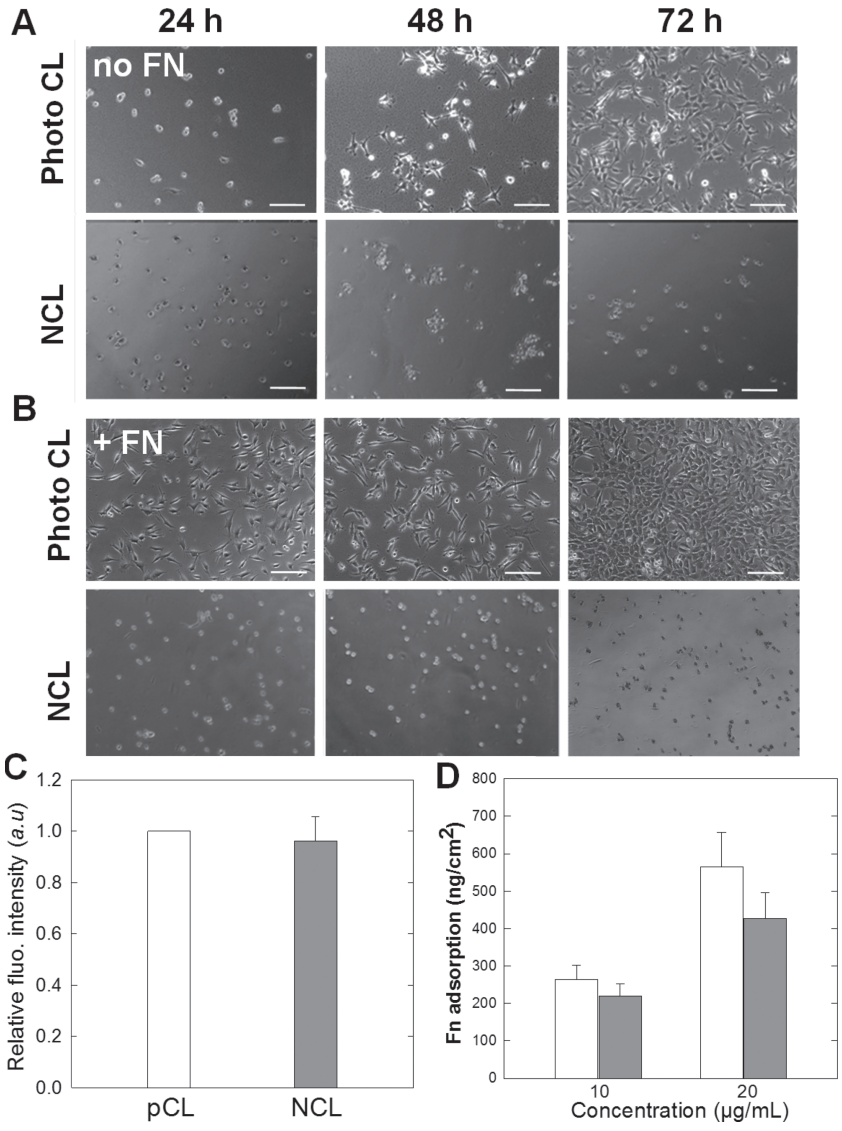

Figure 1. C2C12 myoblast growth on non-crosslinked and photocrosslinked films without (A) or with adsorbed FN (B). In both cases, myoblasts were cultured for 72 h in growth medium on NCL and photoCL films. Scale bar: 100 µm. C) Relative fluorescence intensity of FN-FITC adsorbed onto UCL films as compared photoCL films ones. D) Quantification of fibronectin adsorption by means of fluorescence spectroscopy. FN-FITC was adsorbed at 10 and 20 µg/mL. PhotoCL films (pCL, white bars) and NCL films (gray bars).

the interspacing between the motifs (from 5 to 100 µm) were selected (Table 1). The collective organization of cells on large regions and their behavior in confined conditions were investigated. Cell organization at given time points of 48 h and 72 h in GM for circle and line patterns, respectively, was observed by fluorescence microscopy.

2.3.1. Geometrical Confinement of Cell Clusters on Large Patterns

Cellular assays were first performed on large micro-patterns composed of 100 µm circles separated by a distance of 100 µm to investigate whether cells would be sensitive to these large scale features. The inspection of **Figure 3** shows that myoblasts grew exclusively on stiffer features in agreement with the results obtained previously on homogeneous films of varying stiffness.[36] The restriction in cell adhesion and spreading was visualized by staining the cytoskekelal protein actin. The fraction of cells adhering on stiffer areas compared to the softer background was ≈98% (n = 500 cells), which demonstrates the selectivity of cells for the photo-CL regions. Several cells were contained in a single feature and the limitation of cell extensions at the boundary between photo-CL and NCL areas was clearly seen (Figure 3B). To get more information about the 3D morphology of cell clusters, optical sectioning was performed with a confocal laser scanning microscope allowing 3D reconstruction of cell images (Figure 3C). A color-depth code highlighted the absence of micrometric topography between the substrate and the cells extensions near the boundary of the micropattern (Figure 3C). However cell overgrowth in the vertical direction was observed with heights reaching 9 µm (red zones).

2.3.2. Modification of Cell Protrusive Activity by Subcellular Circular Patterns

Micropatterns corresponding to group 2 (Table 1) were composed of isotropic features with a size smaller than that of an individual cell. They were tested to determine the cell behavior when facing a variation of rigidity below cellular scale. **Figure 4**A shows images of myoblasts grown for 48 h and stained for nuclei, cytoskeletal actin and vinculin. The densities of cells adhering to the films were quantified for each type of micropattern and compared to a homogeneously photoCL film taken as control (Figure 4B). For a given feature size of 5 µm, the cell density decreased when the interspacing increased. Similarly, for a given interspacing of 5 µm, the cell density decreased with the feature size. The fraction of photoCL surface over total surface is given in Figure 4C together with the percentage of spread myoblast cells among adherent cells (spreading being defined as cell deformation with an aspect ratio > 2). About 55% of the cells spread on the 5 µm features independently of the interspacing. However, when the diameter of the photoCL zone was 2 µm, the percentage of spread cells increased from 41 to 69% for an interspacing of 5 and 10 µm, respectively.

A deeper inspection of the protrusions formed by the adherent myoblasts revealed significant morphological responses resulting from the micropatterns (**Figure 5**A–D). Vinculin is a component of focal adhesions, where mechanical force and regulatory signals are conveyed. The presence or absence of recruitment of vinculin to focal adhesion plaques, with consequently increased or decreased formation of focal adhesion

© 2013 WILEY-VCH Verlag GmbH & Co. KGaA, Weinheim

Table 1. Geometrical characteristics of the different patterns. The dimensions are given in µm. The feature sizes are expressed as diameter and line-width for circle and line patterns, respectively.

	Feature shape	Feature size	Feature interspacing	Image
Group 1	Circle	100	100	
Group 2	Circle	5	5	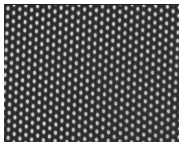
	Circle	5	20	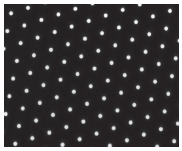
	Circle	2	5	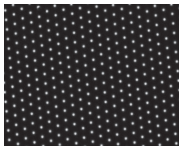
	Circle	2	10	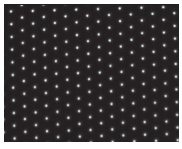
Group 3	Line	20	5	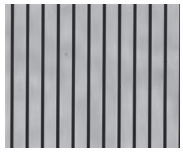
	Line	5	5	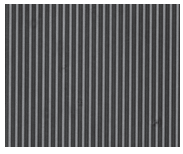
	Line	5	10	
	Line	5	20	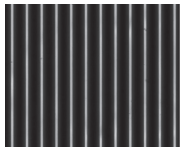

© 2013 WILEY-VCH Verlag GmbH & Co. KGaA, Weinheim

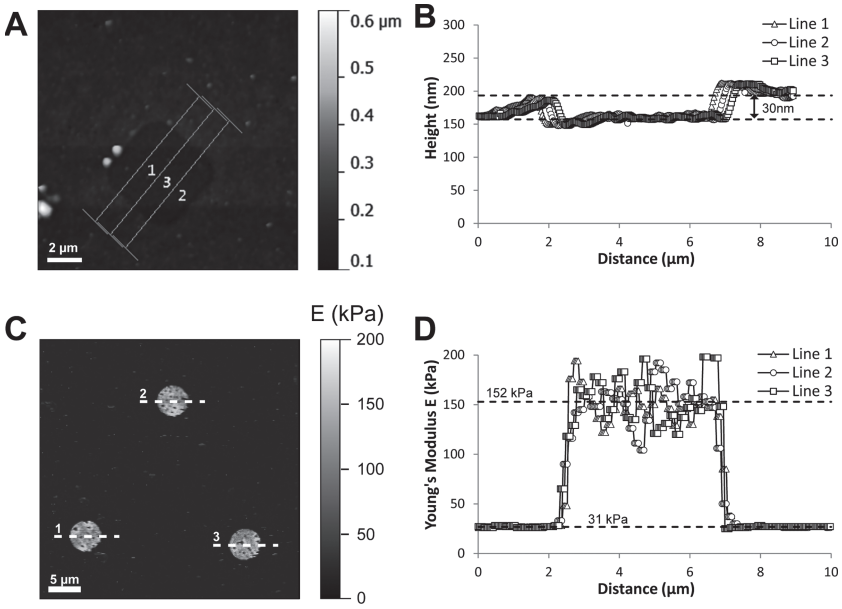

Figure 2. AFM imaging of micropatterned (PLL/HA-VB) films created by photo-crosslinking. A) Topographic image (10 × 10 µm) of a photo-patterned film and B) corresponding topography profile on three different lines. C) Quantitative AFM force mapping of the photopatterned films and D) profiles of the Young's modulus along three different lines. The lines are made across a photo-CL area of 5 µm in diameter.

contacts, gives information about the cell-substrate interaction and the mechano-transduction. Zyxin, a zinc-binding phosphoprotein, is another important component of focal adhesions that has been shown to play a key role in the regulation of actin dynamics, cell migration and is involved in mechano-transduction at cell adhesive structures.[42] Zyxin is usually localized along the cytoskeleton at focal adhesions and accumulate where the cell is exerting traction forces on the substrate during migration.[43] Vinculin staining (Figure 5A) highlighted that the cell extensions adapted to the size of the pattern, with strong dots of fluorescence but no clear plaque (Figure 5A, zoom). Zyxin staining was also diffuse and appeared as punctuate structures, mostly visible on the photoCL (stiffer) areas (Figure 5A). Interestingly, the adhesion points at the tip of the cells were not at the center of the micropatterns but were rather located at the boundaries between stiff and soft parts (Figure 5A, arrowheads). In addition, the staining of the phosphorylated form of the focal adhesion kinase (FAKpY^{397}) emphasized the presence of small focal complexes all over the cell (Figure 5B) instead of large focal adhesions. Of note, the reorganization of the actin cytoskeleton around the photoCL areas was clearly visible, especially around the 2 µm diameter micropatterns (Figure 5C, white arrows). This highlighted the noticeable adjustment of the actin cytoskeleton to the mechanical properties of the substrate.

Quantification of the number of cell protrusions (i.e. large cell extensions) revealed differences between micropatterns (Figure 5D). For a given feature size of 2 or 5 µm, the number of protrusions decreased when the interspacing increased. This variation was more drastic for the 2 µm diameter micropatterns. Moreover, for a given interspacing of 5 µm, the number of protrusions increased when the feature size decreased from 5 to 2 µm. Indeed, an average of ≈7 protrusions/cell was quantified on 5 µm diameter micropatterns with 5 µm spacing, whereas the value increased to 12 protrusions/cell on 2 µm diameter micropatterns and 5 µm spacing. Only 3 and 4 protrusions/cell were counted on the micropatterns with 20 µm and 10 µm spacing, respectively. Thus, the presence of subcellular features of higher rigidity distributed in a softer background impacts significantly the morphology as well as the adhesive structures formed by the myoblast during attachment.

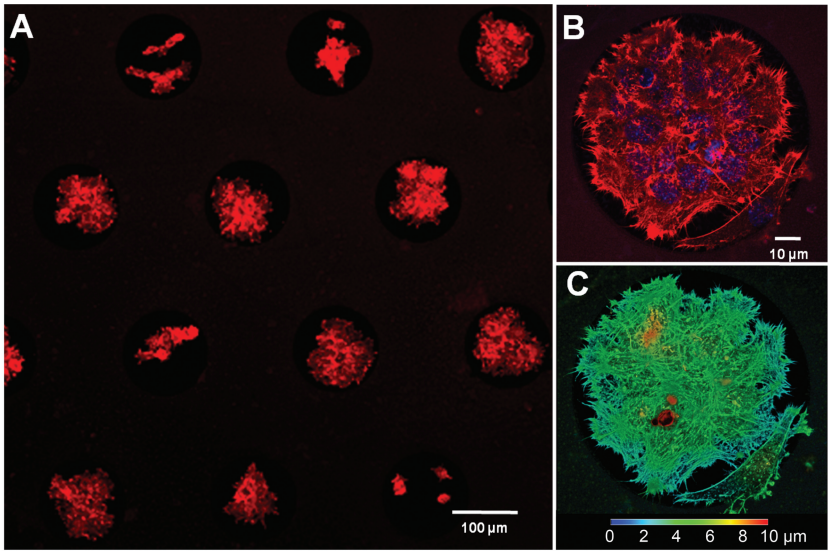

Figure 3. Confinement of C2C12 myoblasts in large circular patterns of photoCL (PLL/HA-VB) films. Myoblasts were cultured for 48 h in growth medium on circular patterns of 100 µm in diameter. Cytoskeletal actin (red) and nucleus (Hoechst, blue) were stained. The images were taken with a 20× objective (A) and a 63× oil immersion objective (B,C) using a confocal laser scanning microscope. C) Color depth coding of the height of the cell cluster shown in (B). Blue is the minimum and red is the maximum at 9 µm.

2.3.3. Alignment and Elongation of Myoblasts on Linear Micropatterns

C2C12 myoblasts are muscle precursor cells that tend to adopt a fibroblastic phenotype and elongate when grown on homogenous substrates.[41] They subsequently fuse into multinucleated myotubes, a process that requires their end-to-end or lateral fusion.[44,45] According to this specific feature of myoblasts, line micropatterns were designed to

© 2013 WILEY-VCH Verlag GmbH & Co. KGaA, Weinheim

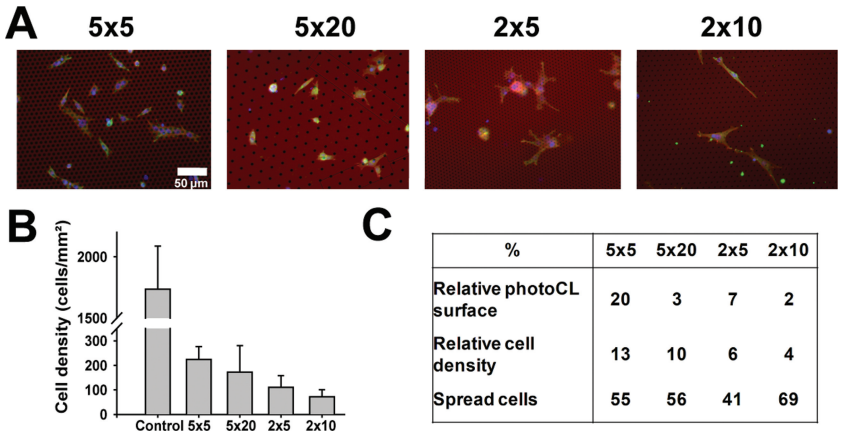

%	5x5	5x20	2x5	2x10
Relative photoCL surface	20	3	7	2
Relative cell density	13	10	6	4
Spread cells	55	56	41	69

Figure 4. Adhesion and spreading of C2C12 myoblasts on anisotropic micropatterns at subcellular scale. Myoblasts were cultured for 48 h in growth medium on circular patterns (diameter (µm) × interspacing (µm): 5 × 5, 5 × 20, 2 × 5 and 2 × 10). A) Fluorescence microscopy images of vinculin (green), actin (red) and nucleus (blue) taken with a 20× objective. The red color of the background is due to the self-fluorescence of the chromium grid embedded into the transparent substrate. B) Cell density on homogeneous photo-CL films (control) and on micropatterns of group 2 (Table 1). C) Table of the relative photo-CL surface of the samples, relative cell density and fraction of spread cells among adherent cells for micropatterns of different sizes.

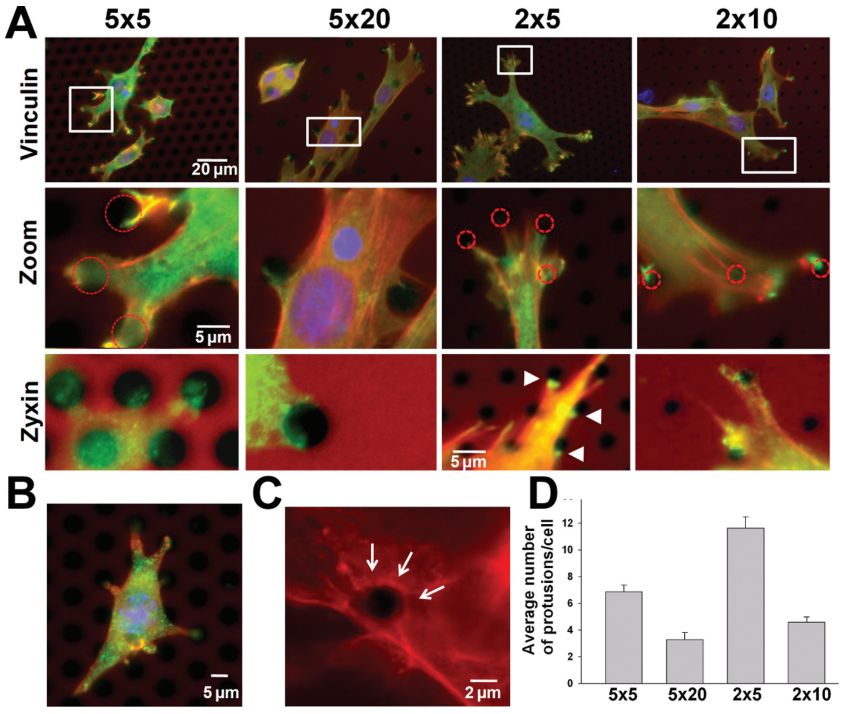

Figure 5. Quantification of protrusive activity of C2C12 myoblasts on subcellular circular micropatterns. Myoblasts were grown for 48 h in growth medium on subcellular circular patterns (same patterns as in Figure 4). A) Fluorescence microscopy images of vinculin or zyxin (green), actin (red) and nucleus (blue) taken with a 63× objective. The second row corresponds to magnified images of the white rectangles of the first raw. The dotted red circles represent the contour of the CL features, when they were not clearly visible. Arrowheads highlight zyxin staining inside the stiff parts of the micropatterns. B) Magnification of a myoblast on the 5 × 5 pattern stained for FAK (green), actin (red) and nucleus (blue). The dots highlighted by FAK staining correspond to focal adhesion plaques. C) Zoom-in image corresponding to actin staining for a cell seeded on a 2 × 10 pattern. Actin reorganization around the circular pattern is highlighted by the white arrows. D) Quantification of the number of protrusions per cell. The values represent data from three independent experiments.

promote cell alignment and to control their orientation. The cells were grown onto micropatterns of group 3 (Table 1) and fixed after 3 days in culture medium (72 h). Their actin cytoskeleton, focal adhesions (vinculin) and nuclei were then stained (**Figure 6**A). Immunostainings showed a very different morphology and adhesion depending on the width and the interspacing of the photoCL stiffer lines (Figure 6). The percentage of aligned cells (Figure 6B), the width of the nuclei (Figure 6C) and their aspect ratio (Figure 6D) were quantified.

On the 20 × 5 micropattern, about 50% of cells were aligned cells (Figure 6B) and ≈50% were spread over several stiffer lines (Figure 6C). It seemed that the 5 µm-softer parts were too small to provide an efficient "barrier" for the cells.

On the 5 × 5 micropattern, the cells crossed the micropatterns and spread all over the surface independently of the rigidity variation. Cell orientation was random and less than 10% of the cells were aligned along the patterned lines (Figure 6B). Thus, a 5 µm-interspacing was not sufficient to restrict cell spreading as cells could step over the NCL stripes. When the width of the micropattern was kept to 5 µm and the interspacing varied between 5 and 20 µm, we noted that more and more cells aligned (Figure 6B) from 24% to 90% for the 5 × 20 µm, where almost all cells aligned along individual stiffer lines (Figure 6A). When the interspacing was 5 or 10 µm, we noted that some cells grew on two adjacent lines or spread over softer regions while keeping most of their focal adhesions on stiffer regions (Figure 6A, pictures taken at higher magnification with 63× objective). Of note, end-to-end cell-cell contacts were also observed when the stiffer parts were separated by 20 µm-wide softer lines. These results highlighted that both the width of the cell adhesive and cell repellent areas are important to direct cell alignment.

Besides cell orientation, we noted significant differences in the width of the nuclei and in its deformation (Figure 6C,D). The 20 × 5 µm micropattern was similar to the control with nuclei of 12 µm in width with an aspect ratio of ≈1.2. Interestingly, a strong decrease of the nucleus width and increase in its aspect ratio was observed for the 5 µm wide stiff lines when the interspacing increased from 5 to 20 µm. The lowest nucleus width of 6 µm and the highest aspect ratio of 3.4 were obtained on the 5 × 20 sample, showing extremely confined and elongated cells in the patterned lines. Thus, controlling cell adhesion

© 2013 WILEY-VCH Verlag GmbH & Co. KGaA, Weinheim

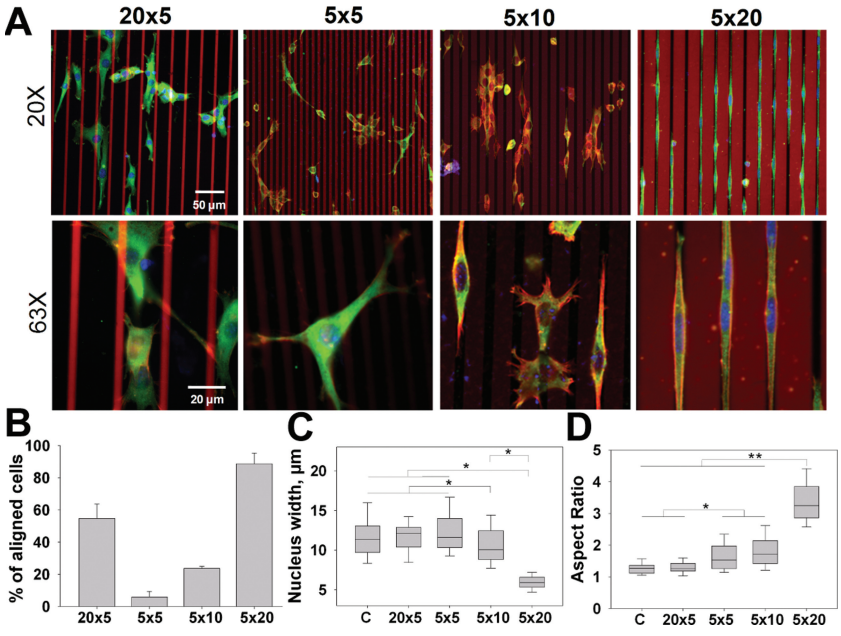

Figure 6. Orientation of C2C12 myoblasts and nuclear shape on linear micropatterns. Myoblasts were cultured for 72 h in growth medium on linear patterns (width of photoCL area (µm) × interspacing (µm): 5 × 5, 5 × 10, 5 × 20 and 20 × 5). A) Fluorescence microscopy images of vinculin (green), actin (red) and nucleus (blue) taken with a 20× objective (upper row) or at higher magnification with a 63× objective (lower row). B) Quantification of the percentage of aligned cells, i.e. cells following the direction of the lines. Quantification of the C) width and D) aspect ratio of the nuclei. $*p < 0.05$ and $**p < 0.001$.

and morphology by a linear micro-pattern of rigidity led to drastic changes in nucleus shape and elongation.

3. Discussion

In this work, we demonstrated that PEM films made of (PLL/HA-VB) can be selectively photo-crosslinked to create spatial arrays composed of stiffer features of various shapes and sizes distributed in a softer background. Various designs of pattern were developed to investigate the collective behavior of the cells on large patterns and the morphology of individual cells at subcellular scale as well. We designed large circular patterns (100 µm) to study multicellular behaviors, subcellular micropatterns (2–5 µm) to examine the local organization of focal adhesions and lines of various widths (5–20 µm) to analyze cellular alignment. This allowed us to follow the stiffness-dependent response of C2C12 myoblasts on PEM films exhibiting a spatially-controlled stiffness.

According to Kawano et al.,[29] five conditions have to be satisfied for studying mechanotaxis: 1) cell-adhesive hydrogel composed of single-chemical components; 2) tunable surface elasticity; 3) ability to produce a sharp elasticity boundary comparable to the size of a single cell; 4) a constant adsorbed density of cell-adhesive protein regardless of the surface elasticity and 5) a smooth topography around the elasticity boundary.

Our photo-crosslinked (PLL/HA-VB) films fulfilled all these conditions, as proved by our previous data,[36] by AFM quantitative force mapping (Figure 2) and by qualitative evaluation of the amount of adsorbed fibronectin (Figure 1). It should be noted that the swelling of the film in the photo-CL regions was minimal, as all the film buildup was done in a physiological solution (i.e., never dried). This leads to a surface-adsorbed thin but swollen hydrogel, whose water content was very high.[46] Indeed, the very small topography of ≈25 nm over a distance of about 600 nm measured between photo-CL and NCL regions corresponded to less than 3% of thickness variation (25 nm over a total film thickness of 1000 nm). Furthermore, the process of photo-crosslinking with the photomask directly embedded into a solid transparent substrate was minimally invasive and allowed to preserve the integrity of the film surface. Finally, AFM images (Figure 2) confirmed that the photo-patterns had a sharp boundary and that their optical resolution was less than 1 µm.

This sharp boundary was far higher than what can be obtained with other techniques and materials. PA gels have mostly been used for creating long range gradients in stiffness extending over several millimeters in length with a smooth transition in Young's modulus (typically few kPa for 100 µm).[17,20] Indeed, these gradients were rather used to investigate cell migration over long distances (millimeter range). The lateral resolution of the boundary was decreased for PDMS to ≈10 µm as compared to ≈100 µm for PA.[24] In all these studies,[17,20,24,26,29] the authors found on long term, over several days, a progressive cell repositioning on the stiffest areas.

Our results of selective adhesion of cells after 3 days on the stiffest part of the films in the presence of large circular patterns (Figure 3), or on the 5 × 10 and 5 × 20 lines (Figure 6), agreed very well with these previous data. When seeded on patterned samples of 100 µm circles, C2C12 myoblasts adhered and proliferated exclusively on photo-CL regions making the photo-CL film a cytophilic surface (98% of the cells) and the NCL background a cytophobic one (Figure 3) with no chemical variation. Cells were clustered into the circular features and the spreading was limited to the photo-CL areas.

Thus, it is interesting to note that very similar long-term phenomena occurred, leading to a differential adhesion, although the materials were different: PA,[17,20,22] PDMS,[23,24] PEG,[26,27] gelatin[29] or PEM films. Indeed, all these substrates were modified or not with different biomacromolecules: collagen in the case of PA, fibronectin in the case of PDMS, RGD peptide or fibrinogen in the case of PEG and no added functionality in the case of gelatin and PEM films. Also, it has to be noted that long term cell culture requires the presence of serum. Thus, some protein adsorption is likely to occur as a function of the time. In the present study, we showed that preincubation with serum-containing medium or with FN did not modify the overall cell response (Figure 1 and Figure SI2, Supporting Information), confirming that protein adsorption is not the major parameter influencing in the cell response.

© 2013 WILEY-VCH Verlag GmbH & Co. KGaA, Weinheim

During photo-CL, a small shrinkage of the film probably occurred, which lead to nanotopographical changes between the photo-CL/NCL parts of ≈25 nm in height. It is now widely acknowledged that substrate nanotopography can regulate various cellular functions, from adhesion, proliferation, migration and differentiation.[47] However, it has to be noted that the relevant feature size studied are rather in the range between 100 nm and 1 μm and that the materials used for such studies are often stiff materials.

Thus, based on the literature on nanotopography, on the literature on influence of substrate stiffness and on our own experimental setup, we believe that substrate stiffness is the most important parameter in our experimental conditions. However, it is not fully possible to exclude any role of the minor topographical change.

It is also interesting to point out that the observed effects, especially the spatial segregation of the cells in the case of some circular and linear patterns, is reminiscent of the effect of chemical micropatterning of substrates on cell adhesion.[48] In the case of chemical micropatterns, however, adhesion occurs usually on the time scale of hours, but the long term maintenance of the micropatterns is less straightforward to achieve.[49] Cell fate was shown to be highly dependent on cell shape[50] implying that the control of the cell microenvironment through engineered surfaces is crucial for fundamental cell-biological studies. Also, the results of cell segregation on the stiffer islands evokes the microwell 3D platforms (see for review),[51] where the goal is to isolate stem cells and to make them grow in well-defined microwells. Using these microarrays to investigate stem cell fate, Lutolf and co-workers demonstrated that physical confinement of cells in 3D microwells led to an increased differentiation of mesenchymal stem cells in adipocytes.[52] The PEM films of patterned rigidity may thus be considered as a "2D niche", which may be useful for futures studies on stem cell behaviors.

On the subcellular anisotropic circular patterns (group 2, Table 1), cells spread over the patterns but cellular extensions were directed toward stiffer parts, as highlighted by vinculin, zyxin and FAKpY^{397} staining (Figure 6A,B). Zyxin is not only a hallmark of mature focal adhesions but also a crucial player in force sensing and force transmission. Zyxin accumulation at the ends of protrusions is an indication of the force exerted by the cells on the film precisely at photoCL areas. However, our observations showed that zyxin, vinculin and FAKpY^{397} were not organized in large focal adhesion plaques but rather in small focal complexes. These observations contrasted with the formation of larger focal adhesions on stiff chemically crosslinked (PLL/HA) films.[53] Besides, protrusive activity of the cells was shown to depend on the geometry of the micropatterns (Figure 6D).

The linear patterns are interesting for the in vitro study of the first steps of myoblast cell orientation and elongation, prior to their fusion. Coordinated cell alignment plays a key role in the formation of functional skeletal myofibers.[45] Therefore, it is one of the major aims of skeletal muscle tissue engineering to recreate in vitro aligned assemblies of myoblasts to drive their subsequent fusion and differentiation in multinucleated polarized myotubes.[54] Myoblast elongation and orientation were previously studied by microgrooving[55] or by chemical micropatterning of a polystyrene substrate.[56] Nanotopography was also shown to influence myoblast fusion.[44] When the substrate is micro- or nanostructured, cell shape and cell orientation are driven by contact guidance and predominantly depends on the width[57] and the height of the grooves.[58] Here, our results using parallel stiff lines distributed in a soft background showed that, by appropriate choice of the line dimensions for the photo-CL versus NCL parts, it was possible to align cells along the patterned lines and to deform strongly their nuclei. Such strong nuclear deformation is reminiscent of what has been recently observed on fibronectin micropatterns and microstructured substrates, where cell nuclei strongly deformed when the cells spread or elongate, leading to many initial gene changes and down-regulation of gene response.[59] Very interestingly, we also observed a sensitivity and selectivity of the cell adhesion toward the stiffer part, when the width of the soft interspacing was large enough to avoid cells to step over the stripes.

The photo-CL PEM films are chemically homogeneous and naturally cell adhesive without the need for additional biochemical functionalization. These films of well-defined width will be used for further studies on the migration and differentiation process of myoblasts in order to understand the important stepss of cell positioning, repositioning, fusion and subsequent differentiation. Moreover, these micropatterns may allow further studies of the effect of the geometrical environment on cellular processes like neurons alignment or hepatocytes colony formation.

4. Conclusions

Cells are sensitive to the rigidity of their micro-environment and especially to the spatial organization of the rigidity. Mechanical gradients or patterns not only regulate adhesion, migration and differentiation of single cells in vivo but also play a strong role in multicellular processes, such as embryogenesis or tumorogenesis. Here, we designed PEM films made of biocompatible PLL and of a photo-reactive HA that can be photo-crosslinked trough a photomask to create spatial patterns of rigidity. The difference in rigidity between the photo-CL parts and the UCL ones is ≈100 kPa. The chemical homogeneity and very minor nanotopography of the films after photo-CL allowed us to highlight the importance of the mechanical signal on the cell behavior. Cellular assemblies were confined on the stiffer areas on 100 μm wide circular micropatterns. Conversely, when the rigidity pattern was at the subcellular scale, cells responded by forming protrusions. This process depended on the geometrical dimensions of the micropattern. Finally, when linear patterns of rigidity were formed, myoblasts aligned and their nuclei were drastically elongated in specific conditions. Such PEM films constitute an innovative tool to control cell shape and subsequently cell fate. In the future, we plan to further investigate the process of cell migration and cell fusion on normal and pathological myoblasts.

5. Experimental Section

Materials and Reagents: Cell culture reagents were from Gibco (Invitrogen, Gibco, Invitrogen, Cergy-Pontoise, France). Fetal bovine serum (FBS) and horse serum (HS) were purchased from PAA

© 2013 WILEY-VCH Verlag GmbH & Co. KGaA, Weinheim

Laboratories (Les Mureaux, France). The antibodies anti-vinculin (V9131), anti-FAKpY^{397}(44624G) and rhodamine phalloidin (P2141) were purchased from Sigma. The anti-zyxin antibody (307011) was purchased from Synaptic System (Goettingen, Germany). Alexa Fluor 488 conjugated antibodies, Hoechst 33342 and the ProLong antifade Gold reagent were purchased from Molecular Probes-Invitrogen (France). All the other reagents were purchased from Sigma and used as received. Hyaluronic acid (HA, 400 000) was supplied by Lifecore Biomedical (Cheska, Minesota, USA). HA-VB derivative modified by 37% of 4-vinylbenzyl (VB) groups was synthesized as previously described.[36]

Fabrication of Transparent Substrates Incorporating a Photomask: Transparent substrates incorporating a metal grid were prepared in a cleanroom environment. The complete micro-fabrication process used to elaborate the substrates requires 4 main steps as described in Scheme S1 (Supporting Information). Briefly, a fused silica slide (Lithosil Q1, Hellma, Germany) was cleaned in a piranha solution [H_2S0_4(98%)/ H_2O_2 50/50 v:v] for 30 min, rinsed with deionized water and dried at 800 °C for 15 min. Then a 1.4 µm-thick negative photoresist layer (AZ 5214E) was spin-coated (4000 rpm, 30 s) on the substrate. After soft baking (110 °C for 1 min), the coated substrate was exposed to UV irradiation for 1.8 s through a photomask (Compugraphics) with a desired pattern design. After an additional soft baking (120 °C for 2 min), the photomask was removed and the coated substrate was fully exposed to the UV light for 6 s. After development (TMAH developer solution), the areas exposed in the first step remained on the substrate. A Reactive Ion Etching (RIE) was performed with $CHCF_3$ gas to form a 100 nm-deep grid on the surface of the fused silica substrate. After an additional brief oxygen plasma etching (1 W for 1 min), a chromium layer of a thickness of 100 nm was deposited in the etched recesses. A lift-off was subsequently performed to remove residual resist parts by immersing the sample in a beaker containing pure acetone and by placing it in an ultrasonic bath for 2 min. The sample was thoroughly rinsed with pure acetone then dried. The modified surface was subsequently spin-coated (2000 rpm, 1 min) by a very thin layer of HSQ resin (FOX-12), which after a rapid thermal annealing (800 °C for 30 min) transformed to a silicon oxide layer covering the whole modified surface of the sample. The inspection of the morphology of the resulting surface by AFM revealed a height variation lower than 20 nm. Substrates with various pattern geometries (circle, square, line) were prepared according to this process.

Film Buildup and Photo-Crosslinking: The films were prepared as previously described[37] with an automated dipping machine (Dipping Robot DR3, Kierstein GmbH, Germany) on fused silica samples for patterned films or 14 mm-diameter glass slides (VWR Scientific, France) for fully exposed films. PLL at 0.5 mg mL^{-1}, HA-VB at 1 mg mL^{-1} and polyethyleneimine (PEI, as precursor layer) at 2 mg mL^{-1} were dissolved in a Hepes-NaCl buffer (0.15 M NaCl, pH 7.4). During $(PLL/HA\text{-}VB)_{12}$ film buildup, all the rinsing steps were performed with a rinsing buffered solution (0.15 M NaCl, pH 6.5). HA-VB solution was stored in the dark to avoid any photo-crosslinking of polyelectrolyte chains.

For the cell culture assays, films deposited onto solid substrates were introduced into 24-well plates and were stored at 4 °C. Multilayers were crosslinked directly in buffer solution by exposure at a distance of 5 cm to a model VL-215.LC (Vilber Lourmat) short-wave ultraviolet lamp (30 W) transmitting at 254 nm.

AFM Characterization of the Film: AFM experiments were performed using a PicoPlus microscope (Agilent Technologies) equipped with a 100-µm scanner in the intermittent-contact mode and a BioCatalyst (Bruker Corporation) equipped with a 150 µm scanner for quantitative nanomechanical mapping. The analyses were realized at ambient temperature in 0.15 M NaCl solution (pH 7.4). A type I MAC lever (Agilent Technologies) with a magnetic coating covering the backside of the cantilever was used. The resonance frequency of the cantilever was ≈45 kHz in water and its nominal spring constant of 0.11 N m^{-1}. For quantitative nanomechanical mapping, we used a DNP-10 cantilever with a resonance frequency of 65 kHz and a spring constant of 0.35 N m^{-1}. The analysis of the images was performed using Image J software v1.47d (NIH, Bethesda).

C2C12 Myoblast Culture and Plating: C2C12 cells (from ATCC, <20 passages) were maintained in Petri dishes in a 37 °C, 5% CO_2 incubator, and cultured in a 1:1 Dulbecco's Modified Eagle Medium (DMEM)/ Ham's F12 medium (growth medium, GM) supplemented with 10% FBS, containing 100 U mL^{-1} penicillin G and 100 µg mL^{-1} streptomycin. Cells were subcultured prior to reaching 60–70% confluence (approximately every 2 days). For cell culture on the $(PLL/HA\text{-}VB)_{12}$ films, cells were seeded at 40 000 cells cm^{-2} in GM. To assess HA-VB cytotoxicity of non crosslinked HA-VB, the cells were grown 4 h with 0.05, 0.1, 0.25 and 0.5 mg of soluble HA-VB diluted in GM. Phase contrast images were taken using an Axiovert 200M (Zeiss, Germany).

Fluorescent Labeling of Intracellular Proteins and Nuclei: For staining of vinculin, zyxin or FAK, cells were fixed in 3.7% formaldehyde in PBS for 20 min and permeabilized for 4 min in TBS (0.15 M NaCl, 50 mM Tris-HCl, pH 7.4) containing 0.2% Triton X-100. Samples were blocked in TBS containing 0.1% BSA for 1 h, and were then incubated with mouse anti-vinculin (1:400) and mouse anti-zyxin (1:1000) antibodies in TBS with 0.2% gelatin for 30 min. AlexaFluor488-conjugated secondary antibody was then incubated for 30 min. For actin staining cells were incubated 30 min with phalloidin-rhodamine (1:800). Nuclei were stained with Hoechst 33342 at 5 µg mL^{-1} for 10 min at room temperature. All the samples were mounted onto coverslips with Prolong antifade reagent and viewed under a fluorescence microscope (Axiovert 200M, Zeiss, Germany or Zeiss LSM 700 for confocal images). Images were acquired with Metaview software using a CoolSNAP EZ CCD camera (both from Ropper Scientific, Evry, France).

Fibronectin Adsorption and Quantification: FITC labeled fibronectin solution was prepared with a concentration of 10 µg mL^{-1} in 0.15 M NaCl solution at physiological pH. NCL and photoCL $(PLL/HAVB)_{12}$ homogeneous films prepared on 14 mm glass slides were incubated with 200 µL of this solution for 1 h at 37 °C. This was followed by gentle rinsing twice with 0.15 M NaCl solution to remove the unabsorbed or loosely attached FN. After this, samples were imaged with a CLSM microscope (Zeiss LSM 700, Germany) and Image J software v1.43m (NIH, Bethesda) was used to measure the fluorescence intensity profiles. For quantification by fluorescence spectroscopy, the (PLL/HA-VB)12 films were built in 96 well plates and 50 µL of FN-FITC was added to each well.

Image Analysis and Statistics: All image quantifications were performed using Image J software v1.43m (NIH, Bethesda). The aspect ratios were determined by dividing the length of nuclei by their width. The results represent three independent experiments. More than 50 nuclei were analyzed for each condition. Data are reported as mean ± standard error of the mean, and statistical comparisons using SigmaPlot software were performed by All Pairwise Multiple Comparison Procedures (Dunn's Method). Statistically different values are reported on the figures ($p < 0.05$ was considered significant).

Supporting Information

Supporting Information is available from the Wiley Online Library or from the author.

Acknowledgements

Prof. B. Nysten (UCL) is thanked for his technical help with AFM measurements. Dr A. Rai and C. Burhin (UCL) are thanked for their technical help with transparent substrate fabrication. The authors thank A. Cavalcanti-Adam for fruitful discussion. This research was performed within the framework of the International Doctoral School in Functional Materials funded by the ERASMUS MUNDUS Program of the European Commission. K.G. benefits from a "M.I.S - Mandat ULYSSE" from the Belgium F.R.S. FNRS. C.P. and K.G. thanks the French-Belgium PHC Tournesol program (EGIDE, N° 26595ZJ). C.P. wishes to thank the European Commission for support in the framework of FP7 via an ERC Starting grant 2010 (GA 259370, BIOMIM) and Grenoble Institute of Technology for a BQR contract 2010.

Received: December 4, 2012
Published online: February 7, 2013

© 2013 WILEY-VCH Verlag GmbH & Co. KGaA, Weinheim

[1] B. Geiger, J. P. Spatz, A. D. Bershadsky, *Nat. Rev. Mol. Cell Biol.* **2009**, *10*, 21–33.
[2] D. Choquet, D. P. Felsenfeld, M. P. Sheetz, *Cell* **1997**, *88*, 39–48.
[3] N. Yamamura, R. Sudo, M. Ikeda, K. Tanishita, *Tissue Eng.* **2007**, *13*, 1443–1453.
[4] M. J. Paszek, N. Zahir, K. R. Johnson, J. N. Lakins, G. I. Rozenberg, A. Gefen, C. A. Reinhart-King, S. S. Margulies, M. Dembo, D. Boettiger, D. A. Hammer, V. M. Weaver, *Cancer Cell* **2005**, *8*, 241–254.
[5] A. J. Day, G. D. Prestwich, *J. Biol. Chem.* **2002**, *277*, 4585–4588.
[6] S. Nemir, H. N. Hayenga, J. L. West, *Biotechnol. Bioeng.* **2010**, *105*, 636–644.
[7] R. J. Pelham, Y. L. Wang, *Proc. Natl. Acad. Sci. USA* **1998**, *95*, 12070–12070.
[8] C. M. Lo, H. B. Wang, M. Dembo, Y. L. Wang, *Biophys. J.* **2000**, *79*, 144–152.
[9] A. J. Engler, M. A. Griffin, S. Sen, C. G. Bonnetnann, H. L. Sweeney, D. E. Discher, *J. Cell Biol.* **2004**, *166*, 877–887.
[10] A. J. Engler, S. Sen, H. L. Sweeney, D. E. Discher, *Cell* **2006**, *126*, 677–689.
[11] A. S. Rowlands, P. A. George, J. J. Cooper-White, *Am. J. Physiol. Cell Physiol.* **2008**, *295*, C1037–C1044.
[12] B. Trappmann, J. E. Gautrot, J. T. Connelly, D. G. Strange, Y. Li, M. L. Oyen, M. A. Cohen Stuart, H. Boehm, B. Li, V. Vogel, J. P. Spatz, F. M. Watt, W. T. Huck, *Nat. Mater.* **2012**, *11*, 642–649.
[13] T. Yeung, P. C. Georges, L. A. Flanagan, B. Marg, M. Ortiz, M. Funaki, N. Zahir, W. Y. Ming, V. Weaver, P. A. Janmey, *Cell Motil. Cytoskeleton* **2005**, *60*, 24–34.
[14] L. A. Flanagan, Y. E. Ju, B. Marg, M. Osterfield, P. A. Janmey, *Neuroreport* **2002**, *13*, 2411–2415.
[15] A. A. Chen, S. R. Khetani, S. Lee, S. N. Bhatia, K. J. Van Vliet, *Biomaterials* **2009**, *30*, 1113–1120.
[16] a) M. Ghibaudo, A. Saez, L. Trichet, A. Xayaphoummine, J. Browaeys, P. Silberzan, A. Buguin, B. Ladoux, *Soft Matter* **2008**, *4*, 1836–1843; b) X. L. Peng, J. Y. Huang, C. Y. Xiong, J. Fang, *J. Biomech.* **2012**, *45*, 116–122.
[17] J. R. Tse, A. J. Engler, *PLOS One* **2011**, *6*. e15978.
[18] F. Guilak, V. C. Mow, *J.Biomechanics* **2000**, *33*, 1663–1673.
[19] R. Liu, A. Schindeler, D. G. Little, *J. Musculoskelet. Neuronal Interact.* **2010**, *10*, 71–76.
[20] B. C. Isenberg, P. A. DiMilla, M. Walker, S. Kim, J. Y. Wong, *Biophys. J.* **2009**, *97*, 1313–1322.
[21] J. G. Jacot, S. Dianis, J. Schnall, J. Y. Wong, *J. Biomed. Mater. Res. Part A* **2006**, *79A*, 485–494.
[22] J. Y. Wong, A. Velasco, P. Rajagopalan, Q. Pham, *Langmuir* **2003**, *19*, 1908–1913.
[23] S. Y. Chou, C. M. Cheng, P. R. Leduc, *Biomaterials* **2009**, *30*, 3136–3142.
[24] D. S. Gray, J. Tien, C. S. Chen, *J. Biomed. Mater. Res. A* **2003**, *66A*, 605–614.
[25] L. Trichet, J. Le Digabel, R. J. Hawkins, R. K. Vedula, M. Gupta, C. Ribrault, P. Hersen, R. Voituriez, B. Ladoux, *Proc. Natl. Acad. Sci. USA* **2012**, *109*, 6933–6938.
[26] J. A. Burdick, A. Khademhosseini, R. Langer, *Langmuir* **2004**, *20*, 5153–5156.
[27] M. S. Hahn, J. S. Miller, J. L. West, *Adv. Mater.* **2006**, *18*, 2679-+.
[28] Y. K. Cheung, E. U. Azeloglu, D. A. Shiovitz, K. D. Costa, D. Seliktar, S. K. Sia, *Angew. Chem. Int. Ed.* **2009**, *48*, 7188–7192.
[29] T. Kawano, S. Kidoaki, *Biomaterials* **2011**, *32*, 2725–2733.
[30] G. Decher, J. D. Hong, J. Schmitt, *Thin Solid Films* **1992**, *210*, 831–835.
[31] J. J. Harris, P. M. DeRose, M. L. Bruening, *J. Am. Chem. Soc.* **1999**, *121*, 1978–1979.
[32] M. D. Moussallem, S. G. Olenych, S. L. Scott, T. C. S. Keller, J. B. Schlenoff, *Biomacromolecules* **2009**, *10*, 3062–3068.
[33] M. T. Thompson, M. C. Berg, I. S. Tobias, M. F. Rubner, K. J. Van Vliet, *Biomaterials* **2005**, *26*, 6836–6845.
[34] L. Richert, F. Boulmedais, P. Lavalle, J. Mutterer, E. Ferreux, G. Decher, P. Schaaf, J. C. Voegel, C. Picart, *Biomacromolecules* **2004**, *5*, 284–294.
[35] S. C. Olugebefola, S. W. Ryu, A. J. Nolte, M. F. Rubner, A. M. Mayes, *Langmuir* **2006**, *22*, 5958–5962.
[36] C. Pozos-Vazquez, T. Boudou, V. Dulong, C. Nicolas, C. Picart, K. Glinel, *Langmuir* **2009**, *25*, 3556–3563.
[37] A. Schneider, G. Francius, R. Obeid, P. Schwinte, J. Hemmerle, B. Frisch, P. Schaaf, J. C. Voegel, B. Senger, C. Picart, *Langmuir* **2006**, *22*, 1193–1200.
[38] K. F. Ren, T. Crouzier, C. Roy, C. Picart, *Adv. Funct. Mater.* **2008**, *18*, 1378–1389.
[39] K. J. M. Boonen, K. Y. Rosaria-Chak, F. P. T. Baaijens, D. W. J. van der Schaft, M. J. Post, *Am. J. Physiol. Cell Physiol.* **2009**, *296*, C1338-C1345.
[40] H. W. Chien, T. Y. Chang, W. B. Tsai, *Biomaterials* **2009**, *30*, 2209–2218.
[41] Y. Ohtake, H. Tojo, M. Seiki, *J. Cell Sci.* **2006**, *119*, 3822–3832.
[42] H. Hirata, H. Tatsumi, M. Sokabe, *J.Cell Sci.* **2008**, *121*, 2795–2804.
[43] a) B. E. Drees, K. M. Andrews, M. C. Beckerle, *J. Cell Biol.* **1999**, *147*, 1549–1559; b) K. Kulangara, Y. Yang, J. Yang, K. W. Leong, *Biomaterials* **2012**, *33*, 4998–5003.
[44] P. Clark, G. A. Dunn, A. Knibbs, M. Peckham, *Int. J. Biochem. Cell Biol.* **2002**, *34*, 816–825.
[45] M. Peckham, *J. Microsc.* **2008**, *231*, 486–493.
[46] T. Crouzier, C. Picart, *Biomacromolecules* **2009**, *10*, 433–442.
[47] D. H. Kim, P. P. Provenzano, C. L. Smith, A. Levchenko, *J. Cell Biol.* **2012**, *197*, 351–360.
[48] R. S. Kane, S. Takayama, E. Ostuni, D. E. Ingber, G. M. Whitesides, *Biomaterials* **1999**, *20*, 2363–2376.
[49] J. Fink, M. Thery, A. Azioune, R. Dupont, F. Chatelain, M. Bornens, M. Piel, *Lab Chip* **2007**, *7*, 672–680.
[50] a) R. McBeath, D. M. Pirone, C. M. Nelson, K. Bhadriraju, C. S. Chen, *Dev. Cell* **2004**, *6*, 483–495; b) C. S. Chen, M. Mrksich, S. Huang, G. M. Whitesides, D. E. Ingber, *Science* **1997**, *276*, 1425–1428.
[51] S. Kobel, M. P. Lutolf, *Biotechniques* **2010**, *48*, IX-XXII.
[52] S. Gobaa, S. Hoehnel, M. Roccio, A. Negro, S. Kobel, M. P. Lutolf, *Nat. Methods* **2011**, *8*, 949–955.
[53] K. F. Ren, L. Fourel, C. G. Rouviere, C. Albiges-Rizo, C. Picart, *Acta Biomater.* **2010**, *6*, 4238–4248.
[54] J. Stern-Straeter, F. Riedel, G. Bran, K. Hormann, U. R. Goessler, *In Vivo* **2007**, *21*, 435–444.
[55] a) J. L. Charest, A. J. Garcia, W. P. King, *Biomaterials* **2007**, *28*, 2202–2210; b) M. T. Lam, S. Sim, X. Zhu, S. Takayama, *Biomaterials* **2006**, *27*, 4340–4347; c) K. Shimizu, H. Fujita, E. Nagamori, *Biotechnol. Bioeng.* **2009**, *103*, 631–638.
[56] a) P. Bajaj, B. Reddy, L. Millet, C. N. Wei, P. Zorlutuna, G. Bao, R. Bashir, *Integr. Biol.* **2011**, *3*, 897–909; b) E. Serena, S. Zatti, E. Reghelin, A. Pasut, E. Cimetta, N. Elvassore, *Integr. Biol.* **2010**, *2*, 193–201.
[57] a) X. Lu, Y. Leng, *J. Biomed. Mat. Res. B* **2009**, *90B*, 438–445; b) C. Monge, K. Ren, R. Guillot, K. Berton, D. Peyrade, C. Picart, *Tissue Eng.* **2012**.
[58] Y. Zhao, H. Zeng, J. Nam, S. Agarwal, *Biotechnol. Bioeng.* **2009**, *102*, 624–631.
[59] a) M. Versaevel, T. Grevesse, S. Gabriele, *Nat. Com.* **2012**, *3*; b) M. J. Dalby, M. O. Riehle, S. J. Yarwood, C. D. W. Wilkinson, A. S. G. Curtis, *Exp. Cell Res.* **2003**, *284*, 274–282; c) P. M. Davidson, H. Ozcelik, V. Hasirci, G. Reiter, K. Anselme, *Adv. Mater.* **2009**, *21*, 3586–3590+.

© 2013 WILEY-VCH Verlag GmbH & Co. KGaA, Weinheim